Influence of Sequential Solvation on Metal-to-Ligand Charge Transfer in Bis(2,2′,2″-terpyridyl)iron(II) Clustered with Dimethyl Sulfoxide

Thomas G. Spence,† Brett T. Trotter, and Lynmarie A. Posey*

Department of Chemistry, Vanderbilt University, Box 1822, Station B, Nashville, Tennessee 37235

Received: June 2, 1998

The first direct measurements of the contributions of individual solvent molecules to solvent reorganization associated with photoinitiated charge transfer in a coordination complex are reported for gas-phase clusters of bis(2,2′,2″-terpyridyl)iron(II), $[Fe(terpy)_2]^{2+}$, with dimethyl sulfoxide (DMSO) prepared by electrospray ionization. Excitation of $[Fe(terpy)_2 \cdot (DMSO)_n]^{2+}$ clusters at wavelengths corresponding to the metal-to-ligand charge-transfer (MLCT) absorption characteristic of Fe(II)−polypyridine complexes in solution triggers evaporation of solvent molecules, permitting the application of laser photofragmentation mass spectrometry to monitor MLCT absorption. The energy of the optical transition corresponding to MLCT E_{op} is reported for $[Fe(terpy)_2 \cdot (DMSO)_n]^{2+}$ clusters ($n = 1-11$), and the cluster-size dependence of E_{op} is examined following Jortner's cluster-size-equation approach (Jortner, J. *Z. Phys. D* **1992**, *24*, 247). The first 11 DMSO molecules contribute 54−63% of the bulk solvent reorganization energy, based on estimates that E_{op} for the gas-phase $[Fe(terpy)_2]^{2+}$ complex falls between 1.860×10^4 and 1.876×10^4 cm^{-1}.

Introduction

Optical electron-transfer (ET) processes in coordination complexes, particularly metal-to-ligand charge transfer (MLCT) and metal-to-metal charge transfer (MMCT), have been studied extensively.[1−3] Typically, solvent reorganization is probed by changing the composition of the bulk solvent and then measuring the energy of the optical transition E_{op}, which corresponds to the maximum of the charge-transfer (CT) absorption band. In fact, E_{op} is generally partitioned into contributions from the zero-point energy difference between the ground and excited states of the isolated CT chromophore ΔE_o; the inner-sphere reorganization of the chromophore to accommodate the new charge distribution in the CT excited state E_{in}; and the outer-sphere or solvent reorganization in response to the new charge distribution E_{out}, where

$$E_{op} = \Delta E_o + E_{in} + E_{out} \quad (1)$$

In many cases, the solvent reorganization energy correlates strongly with the bulk dielectric properties of the solvent. This relationship between bulk dielectric properties of the solvent and solvent reorganization first emerged from theory[4] developed by Marcus,[5−7] Hush,[8] and Levich and Dogonadze[9−11] for thermal electron transfer (ET). Hush[12,13] subsequently established the connection between thermal and optical ET and extended the theory developed for thermal ET to optical intervalence ET. An alternate approach[14] based on theory developed by Kirkwood[15] to predict the free energy of solvation of ions having an arbitrary charge distribution in a continuous dielectric has also been invoked to interpret the solvent dependence of optical ET.

The simplified description of the interactions between the solute(s) participating in ET and the surrounding medium offered by dielectric continuum models has led to their widespread application. However, it is precisely this oversimplification in the treatment of solute−solvent interactions that results in a breakdown in the ability of these models to make quantitative predictions of E_{op}.[16−19] Fine tuning of dielectric continuum models[20] has improved quantitative agreement between theory and experiment; nevertheless, the underlying assumption that solvent behaves as a dielectric continuum ignores the molecular details of the strongest interactions that occur between the solute and adjacent solvent molecules in the first solvent shell. The response of E_{op} in solvents which exhibit strong, spatially directed interactions, such as hydrogen[21−23] or Lewis acid−base[24−26] bonding with the ET chromophore, highlights the limitations of dielectric continuum models. These local solvent−solute interactions effectively saturate the dielectric immediately surrounding the solute.[16,20,27] A further complication in the behavior of E_{op}, which manifests itself as a concentration dependence, arises from ion pair formation between ionic ET chromophores and counterions present in solution.[17,23,28,29]

Theoretical work has begun to focus on the impact of local interactions between coordination complexes and solvent on the energetics of optical ET. Zerner and co-workers[30] have calculated the MLCT transition energy for the isolated $[Ru(NH_3)_5(pyr)]^{2+}$ complex (pyr = pyridine) as well as for this complex associated with 5, 10, and 15 water molecules using the intermediate neglect of differential overlap (INDO) model at the configuration interaction (CI) level of theory. The addition of water molecules near the five ammine ligands of the complex had dramatic effects on the energies of both the MLCT and the pyridine-localized $\pi \rightarrow \pi^*$ transitions consistent with the solution absorption spectra, which could not be reproduced by a dielectric continuum model. Reimers, Hush, and co-workers have combined ab initio and semiempirical methods with Monte Carlo and molecular dynamics simulations[31−33]

* To whom correspondence should be addressed. E-mail: lynmarie.a.posey@vanderbilt.edu.

† Current address: Department of Chemistry, Stanford University, Stanford, CA 94305.

S1089-5639(98)02468-2 CCC: $15.00
Published on Web 09/15/1998

to model the effects of local solvent−solute interactions, particularly hydrogen bonding, on optical ET. When they applied these methods to predict the MLCT transition energies for $[Ru(NH_3)_5L]^{2+}$, L = pyr or pyrazine (pyz), in water,[34−36] they found that it was only necessary to explicitly determine molecular interactions between the coordination complex and water molecules located within the first solvent shell; solvent beyond the first shell could be modeled as a dielectric continuum.

Experimentally, optical[37−40] and electrochemical[38, 41−43] studies of coordination complexes exhibiting MMCT and MLCT in mixtures of acetonitrile and dimethyl sulfoxide (DMSO) have provided the clearest evidence of the importance of local solvent interactions in ET and the magnitude of their contribution to the solvent reorganization energy. At mole fractions of DMSO below 0.1, E_{op} deviated significantly from the linear dependence on solvent composition anticipated if the composition of the solvent shell immediately surrounding the coordination complexes mirrored bulk solution. This behavior was attributed to preferential solvation of the coordination complexes studied by DMSO in the mixed solvent. Hupp and co-workers[37,39] also concluded that the response of solvent molecules in the first solvent shell to the change in the charge distribution accompanying optical ET accounted for most of the solvent reorganization energy. Although the concentration effects observed with mixed solvents were pronounced, these experiments still have not resolved local contributions to the solvent reorganization energy from the bulk contributions because the coordination complex "clustered" with DMSO remained embedded in a continuum of acetonitrile.

This paper explores the contributions of individual solvent molecules to solvent reorganization *directly* by probing the energy of the $d \rightarrow \pi^*$ MLCT transition in the low-spin[44] bis-(2,2′,2″-terpyridyl)iron(II) complex, $[Fe(terpy)_2]^{2+}$, as a function of solvent number, $n = 1-11$, in gas-phase clusters with DMSO. Clusters not only permit control over the exact number of solvent molecules surrounding the ET chromophore, but they also eliminate the ion pairing with counterions responsible for the ionic-strength dependence of E_{op} in the condensed phase. This work builds upon our previous efforts to develop electrospray ionization as a source of clusters containing transition-metal ions in the +2 oxidation state for spectroscopic study.[45−47]

The $[Fe(terpy)_2]^{2+}$ complex exhibits the $^1MLCT \leftarrow {}^1A_1$ absorption characteristic of Fe^{II}−polypyridines in which the excited electron is initially localized on a single ligand.[14,48] This transition is ideally suited to detection via cluster photofragmentation because, in contrast with the corresponding Ru^{II} and Os^{II} complexes, $[Fe(terpy)_2]^{2+}$ does not emit following excitation to the ^1MLCT excited state.[49] Instead, the ^1MLCT excited-state undergoes rapid intersystem crossing ($\tau < 1$ ps) to form the long-lived $^5T_2$ ligand-field excited state,[50] which has a lifetime of 2.54 ± 0.13 ns in water at 298 K.[51] Note that these generalized state designations for Fe^{II}−polypyridines are based on the symmetry of the ligand field rather than the overall symmetry of the complex. On the basis of transient spectra, which indicated that thermalization of the $^5T_2$ state occurred within 2−3 ps following formation, McCusker et al.[50] proposed that the solvent played an important role as a sink for dissipation of vibrational excitation in the $^5T_2$ state. The remaining excitation energy is dissipated nonradiatively by vibrational relaxation following intersystem crossing from the $^5T_2$ state back to the ground $^1A_1$ state. When $[Fe(terpy)_2]^{2+}$ is isolated in gas-phase clusters, excitation of the MLCT transition triggers cluster photofragmentation

$$[Fe^{II}(terpy)_2\cdot(DMSO)_n]^{2+} + h\nu \rightarrow [Fe^{III}(terpy^-)(terpy)\cdot(DMSO)_n]^{2+}* \quad (2)$$

$$[Fe^{III}(terpy^-)(terpy)\cdot(DMSO)_n]^{2+}* \rightarrow [Fe^{II}(terpy)_2\cdot(DMSO)_m]^{2+} + (n-m)DMSO \quad (3)$$

As a consequence, the wavelength-dependent photodepletion action spectra reflect cluster absorption.

Experimental Section

The tandem mass spectrometer[46] equipped with an electrospray ionization (ESI) cluster source[47] used to collect laser photodepletion action spectra was described in detail previously. Briefly, ESI of a 1.5×10^{-4} M methanolic solution (Fisher, Certified ACS) of $Fe(terpy)_2(PF_6)_2$ generated gas-phase $[Fe(terpy)_2]^{2+}$ and $[Fe(terpy)_2\cdot(CH_3OH)_n]^{2+}$ ions. The region between the electrospray needle and the metal capillary, which served as the sampling orifice into the tandem mass spectrometer, was gently purged with N_2 saturated with DMSO (Fisher, Certified ACS) or DMSO-d_6 (Cambridge Isotope Laboratories, 99.9% D). Conditions in the ESI source were optimized to remove $[Fe(terpy)_2\cdot(CH_3OH)_n]^{2+}$ clusters formed in the ESI process and to produce $[Fe(terpy)_2\cdot(DMSO)_n]^{2+}$ clusters, which formed from the association of gas-phase ions and neutral solvent molecules in the intermediate pressure regions of the ESI source.[47]

After traversing two stages of differential pumping, the ions entered the collision-free environment of the tandem mass spectrometer. A Wien filter (Colutron Research, model 600-B) selected a particular cluster size from the distribution of clusters generated by ESI. Following mass selection, an electrostatic turning quadrupole[52] deflected the ion beam by 90° and merged it with the output of a tunable ring dye laser (Coherent 899-01, typical line width < 2 GHz) pumped by an argon ion laser (Coherent Innova 420). The laser and ion beams copropagated through a set of electrostatic focusing optics and an 80-cm long quadrupole ion guide. A quadrupole mass filter (Extrel EXM-340 system) located at the exit of the ion guide separated parent cluster ions from photofragment ions. Since the detailed description of this instrument was reported,[46] the electronics for the quadrupole mass filter were upgraded to operate at 0.88 MHz (300 W), which extended the *m/z* range to over 1000. Ions were detected with a conversion dynode and Channeltron electron multiplier (Galileo Electro-Optics model 4870E) and scored with a photon counter. Typically, the signal for mass-selected $[Fe(terpy)_2\cdot(DMSO)_n]^{2+}$ clusters ranged from 1.5×10^4 ions s^{-1} for the $n = 1$ cluster to 1.5×10^3 ions s^{-1} for the $n = 11$ cluster.

Absorption by $[Fe(terpy)_2\cdot(DMSO)_n]^{2+}$ clusters was detected indirectly by monitoring the depletion of the mass-selected cluster ion beam resulting from photofragmentation. Photodepletion action spectra were collected for $[Fe(terpy)_2\cdot(DMSO)_n]^{2+}$ clusters as a function of photon energy over the range $(1.78-1.89) \times 10^4$ cm^{-1} (rhodamine 560 and pyrromethene 556 dyes, Exciton). Pumping the dye laser with the multiline output of the argon ion laser determined the high-energy limit.

In contrast with our previous work,[46] where the yields of photofragment ions were measured at fixed wavelengths spaced by 5−10 nm and then later assembled into photofragmentation action spectra, photodepletion of the mass-selected ion beam was measured as the dye laser was scanned in this study. A

mechanical chopper (Stanford Research Systems SR540) gated the laser at 30 Hz while a photon counter (Stanford Research Systems SR400) registered the amplified signal (Channeltron detector and Stanford Research Systems SR440 preamplifier) from mass-selected parent cluster ions striking the conversion dynode in 10-ms periods. The number of ions detected in each period was sorted based upon the state of the laser beam during the counting period to distinguish photofragmentation from metastable decomposition.[45,46] The ion intensity was sampled for 3500 10 ms periods before average laser-on and laser-off ion intensities were determined and the laser wavelength (Burleigh Wavemeter Jr.) and power (Ophir 10A thermopile detector, DGX display) were recorded. Percent depletion of the ion beam was then calculated from the average laser-on and laser-off ion intensities and normalized with respect to laser power, which was held below 400 mW (91 W cm^{-2}) to avoid saturation of the strong MLCT transition. Wavelength-dependent photodepletion action spectra were generated by stepping the dye laser output in approximately 14 cm^{-1} increments, while performing three to five determinations of the percent depletion of the cluster ions at each step during an individual scan. The data reported represent the average of several of these scans. Scans obtained on different days or using different laser dyes were normalized using overlapping data points to correct for changes in laser and ion beam overlap.

Bis(2,2′,2″-terpyridyl)iron(II), $[Fe(terpy)_2]^{2+}$, was synthesized following the work of Morgan and Burstall[53] from $FeSO_4 \cdot 7H_2O$ (Fisher, 99%) and 2,2′,2″-terpyridine (Aldrich, 98%) and was isolated as a the hexafluorophosphate salt ($NaPF_6$, Aldrich, 98%). The UV−vis absorption spectrum of $[Fe(terpy)_2]^{2+}$ in DMSO was recorded using an Hitachi U-2000 spectrophotometer (wavelength accuracy ± 0.4 nm). The DMSO solution used to obtain the absorption spectrum was prepared immediately before recording the spectrum.

Results

Figure 1 shows the photodepletion action spectra of $[Fe(terpy)_2 \cdot (DMSO)_n]^{2+}$ clusters, $n = 1-11$, which reflect MLCT absorption by the $[Fe(terpy)_2]^{2+}$ complex isolated in gas-phase clusters, and the corresponding solution absorption spectrum ($n \rightarrow \infty$) over the photon energy range (1.78−1.89) × 10^4 cm^{-1}. An overlapping peak in the parent ion mass spectrum necessitated using DMSO-d_6 to prepare the $n = 3$ clusters. Perdeuterated DMSO shifted the peak for the $n = 3$ cluster by $\Delta m/z = 9$ and eliminated the mass coincidence that interfered with collection of the $n = 3$ photodepletion action spectrum. The smooth line through each spectrum represents the nonlinear least-squares fit of the experimental data to a log-normal line shape,[54] which was used to locate the maximum of the asymmetric MLCT band (Table 1). A constant multiplier of +1 or −1 was added to the expression for the "skewness" of the log-normal function to account for its direction and was treated as an adjustable parameter in the fits of experimental data. The skew of the fits shifts from negative to positive at $n = 10$. In general, the photodepletion action spectra of $[Fe(terpy)_2]^{2+}$ clusters shift to the red with increasing cluster size. The anomalous[54] negative skew in the log-normal fits for small clusters results from limited photodepletion data on the blue side of the absorption maximum.

Each spectrum represents an average of at least three scans, and all traces are normalized with respect to the band maximum. Depletion of the $[Fe(terpy)_2 \cdot (DMSO)_n]^{2+}$ cluster ion beam ranged from 8 to 21% at the maximum normalized to 1 W. Variation in the observed maximum percent depletion may be attributed to changes in laser and ion beam overlap and to variation in the amount of time that clusters spend in the laser interaction region. Clusters generated by ESI exit the ion source with the same kinetic energy; therefore, larger clusters spend more time in the laser interaction region of the tandem mass spectrometer. For example, $[Fe(terpy)_2 \cdot (DMSO)_1]^{2+}$ clusters spend ∼150 μs in the laser interaction region, while $[Fe(terpy)_2 \cdot (DMSO)_{11}]^{2+}$ clusters interact with the laser beam for ∼240 μs. The absorption spectrum of $[Fe(terpy)_2](PF_6)_2$ in bulk DMSO solution is shown in Figure 2 for direct comparison with the photodepletion action spectra of $[Fe(terpy)_2 \cdot (DMSO)_n]^{2+}$, $n = 1$ and 8; these spectra reflect the general trend that the energy of the MLCT transition shifts to the red with increasing solvent number.

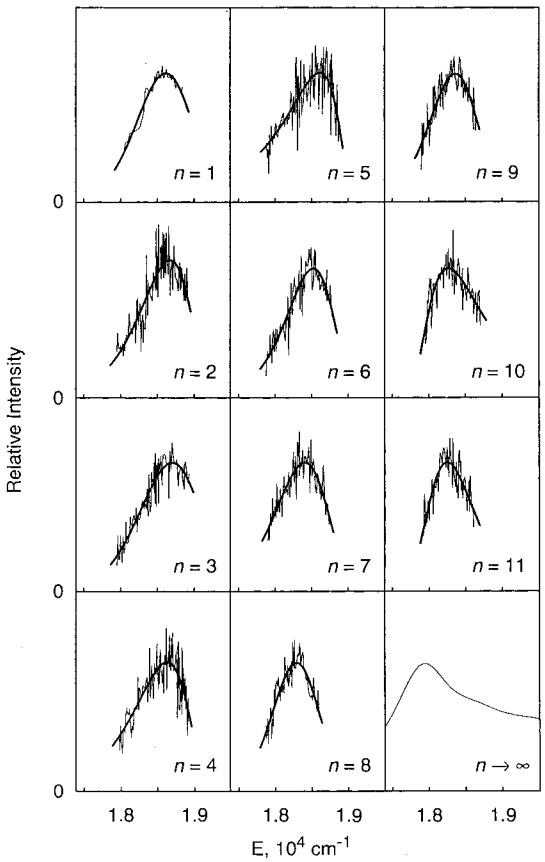

Figure 1. Photodepletion action spectra for $[Fe(terpy)_2 \cdot (DMSO)_n]^{2+}$ clusters, $n = 1-11$, obtained at photon energies in the range (1.78−1.89) × 10^4 cm^{-1}. Note that the spectrum shown for $n = 3$ is the photodepletion action spectrum of $[Fe(terpy)_2 \cdot (DMSO\text{-}d_6)_3]^{2+}$ (see text). The smooth lines through the data represent nonlinear least-squares fits of the data to log-normal functions. The corresponding absorption spectrum of $[Fe(terpy)_2](PF_6)_2$ in DMSO, designated by $n \rightarrow \infty$, is also shown over the same range of photon energies.

Figure 3 shows the position of the band maximum corresponding to E_{op} for MLCT obtained from log-normal fits to the photodepletion action spectra as a function of cluster size, and Table 1 summarizes the experimentally determined band maxima. Error bars represent the standard deviation obtained by fitting individual scans independently. The energy of the MLCT transition increases, moving gradually away from the bulk limit, as the second and third solvent molecules are added and then drops back to roughly the same value observed for $n = 1$ as the fourth and fifth solvent molecules are added. With the addition of the sixth through eighth DMSO solvent molecules, the energy of the MLCT transition rapidly declines from 18616 to 18302 cm^{-1}, beginning the red shift toward the

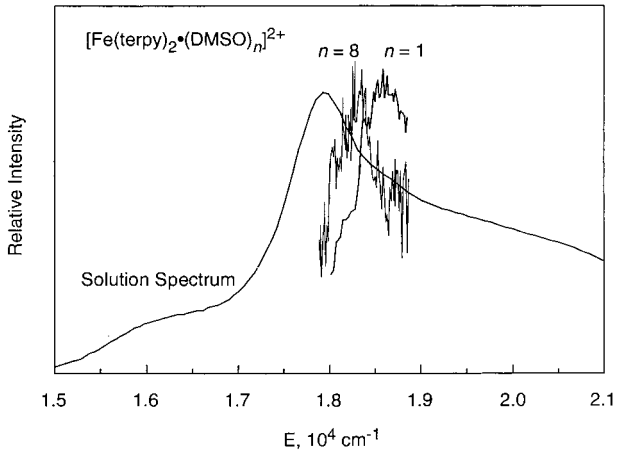

Figure 2. Absorption spectrum of $[Fe(terpy)_2](PF_6)_2$ in DMSO solution at 20 °C shown with the photodepletion action spectra of $[Fe(terpy)_2 \cdot (DMSO)_n]^{2+}$, $n = 1$ and 8. For purposes of comparison, the maxima in the cluster photodepletion spectra are normalized to match the maximum in the solution absorption spectrum.

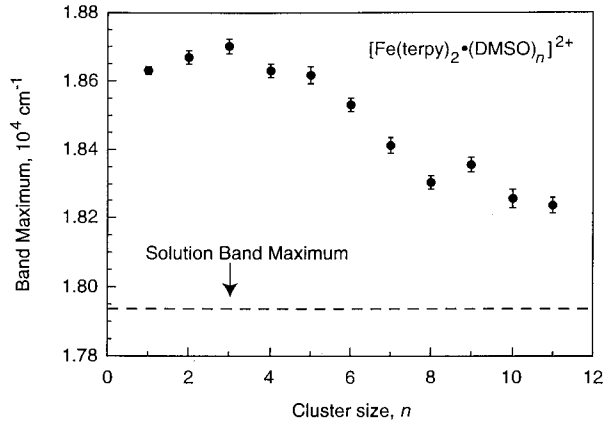

Figure 3. Maxima of the MLCT absorption band of $[Fe(terpy)_2 \cdot (DMSO)_n]^{2+}$ clusters E_{op}, monitored by photodepletion plotted as a function of solvent number, n.

bulk limit. The energy of the transition increases slightly with the addition of the ninth solvent molecule but continues to decrease with the addition of the 10th and 11th DMSO. Comparison of the shift in the band maximum from $n = 5$ to $n = 8$ with the shift from $n = 8$ to $n = 11$ suggests that the contribution of individual DMSO solvent molecules is beginning to level off, which would be expected as the first solvent shell closes.

Discussion

Structure and Spectroscopy of Bis(2,2′,2″-terpyridyl)-iron(II). X-ray crystallography[55] reveals that $[Fe(terpy)_2]^{2+}$ has approximate D_{2d} symmetry, exhibiting axial compression with shorter Fe−N bonds to the central terpyridyl N and longer bonds to the N's of the terminal rings. A space-filling model of $[Fe(terpy)_2]^{2+}$ generated by MacroModel[56] using crystallographic coordinates[55] is shown in Figure 4. Mössbauer spectra[57] suggest that tetragonal distortion of the ligand field arises from strong σ bonding, resulting from donation of electron density from the nonbonding electrons of the ligands' central N's to the unoccupied metal d_{z^2} orbital combined with π back donation of metal d_{xz} and d_{yz} electron density to the unoccupied ligand π^* orbitals. Distortion of the O_h ligand field to D_{2d} symmetry splits the Fe^{II} t_{2g} (b_2, e) and e_g (b_1, a_1) orbitals. The reduced symmetry of the complex also results in splitting of the ligand π^* orbitals.[57]

The solution absorption spectrum of the low-spin $[Fe(terpy)_2]^{2+}$ complex in the region from 15000 to 21000 cm^{-1} consists of several partially overlapping bands (Figure 2). The dominant band in the absorption spectrum of $[Fe(terpy)_2(PF_6)_2]$ in DMSO solution with $\lambda_{max} = 1.793 \times 10^4$ cm^{-1} (Figure 2) is assigned as the $^1MLCT_1 \leftarrow {}^1A_1$ transition from a metal-centered e orbital to the lowest of the ligand-based π^* orbitals. This MLCT transition is the focus of the work reported here. It is lower in energy and narrower than the corresponding transition in the $[Fe(bpy)_3]^{2+}$ complex in DMSO ($\lambda_{max} = 1.896 \times 10^4$ cm^{-1}). The reduction in the MLCT energy in the terpyridyl complex relative to the bipyridyl complex results from enhanced back donation and the more easily reduced[48] extended π system of terpyridine. The narrowness of the band is attributed to the stiffness of the terpyridyl ligand, which restricts the geometry change accompanying MLCT excitation.[58] The broad band located 1200−1500 cm^{-1} to the blue of the maximum corresponds to the MLCT transition to the higher of the split ligand π^* orbitals, $^1MLCT_2 \leftarrow {}^1A_1$;[57, 58] it is also likely that transitions to vibrationally excited levels of the $^1MLCT_1$ state contribute.[58] A shoulder also appears on the red side of the main MLCT absorption band; resonance Raman depolarization ratios[59] indicate that it corresponds to an electronic transition separate from the MLCT transitions. In Fe^{II}−polypyridines, the ligand-field splitting is sufficiently small to drop optically accessible ligand-field excited state(s) below the MLCT excited state. On the basis of the d^6 configuration Tanabe−Sugano energy diagram,[60] we assign this shoulder as the second allowed ligand-field transition ($^1T_2 \leftarrow {}^1A_1$); distortion of the complex from O_h symmetry enhances the strength of this ligand-field absorption.

Cluster-Size Dependence of E_{op} for MLCT in $[Fe(terpy)_2 \cdot (DMSO)_n]^{2+}$ Clusters. Figure 3 summarizes the cluster-size dependence of the energy of the optical transition associated with MLCT E_{op}, and reflects the contributions of individual DMSO molecules to solvent reorganization. We begin by examining the general trend in E_{op} as a function of cluster size before looking at the detailed cluster-size dependence. Comparison of E_{op} for $[Fe(terpy)_2 \cdot (DMSO)_1]^{2+}$ with that for the $[Fe(terpy)_2]^{2+}$ complex in DMSO solution reveals the effect of solvent on the energy of the MLCT transition at a coarse level. The energy of the optical transition shifts by -7.0×10^2 cm^{-1} in going from the cluster with one DMSO molecule to bulk solution. Addition of 10 DMSO molecules to the $[Fe(terpy)_2 \cdot (DMSO)_1]^{2+}$ cluster shifts E_{op} by -4.0×10^2 cm^{-1}, with a shift of -3.0×10^2 cm^{-1} remaining to reach the bulk limit. The shift from $n = 1$ to $n = 11$ accounts for 57% of the red shift between $n = 1$ and the bulk limit.

We rule out cluster temperature as the origin of the general trend of decreasing E_{op} with increasing cluster size upon the basis of our previous analysis of metastable decay fractions for $[Fe(bpy)_3 \cdot (CH_3OH)_n]^{2+}$ clusters ($n = 2-6$) using the evaporative ensemble model and RRK rate constants.[46] Temperatures of the $[Fe(bpy)_3 \cdot (CH_3OH)_n]^{2+}$ clusters deceased from 321 K for the $n = 2$ cluster to 239 K for the $n = 6$ cluster. A similar trend for $[Fe(terpy)_2 \cdot (DMSO)_n]^{2+}$ clusters would produce a slight blue shift in E_{op} with increasing cluster size. Instead, the general trend of decreasing E_{op} with addition of solvent molecules arises from preferential stabilization of a polar MLCT excited state relative to the nonpolar ground state by a polar solvent. A polar excited state results because the electron

TABLE 1: Metal-to-Ligand Charge Transfer Band Maxima in $[Fe(terpy)_2 \cdot (DMSO)_n]^{2+}$ Clusters

n	band maximum, cm^{-1}	n	band maximum, cm^{-1}	n	band maximum, cm^{-1}	n	band maximum, cm^{-1}
1	18629 ± 12	4	18631 ± 19	7	18410 ± 23	10	18256 ± 26
2	18670 ± 19	5	18616 ± 24	8	18302 ± 20	11	18235 ± 23
3	18702 ± 21	6	18529 ± 19	9	18354 ± 22	∞	$(1.793 \pm 0.002) \times 10^4$

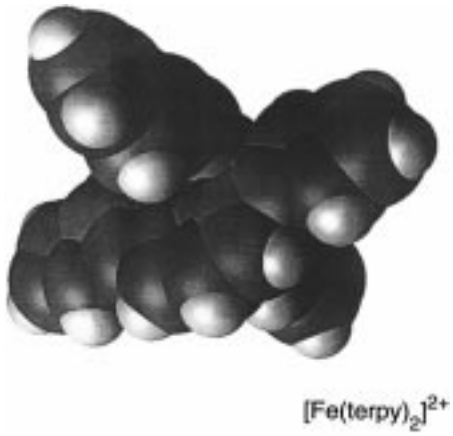

Figure 4. Space-filling model of $[Fe(terpy)_2]^{2+}$ generated by MacroModel[56] using crystallographic coordinates obtained by Baker and Goodwin.[55] The intraligand distance between the centers of the hydrogen atoms bonded to C(4) and C(4″) of the terpyridyl ligands is approximately 13.3 Å, and the interligand distance between the centers of the hydrogen atoms bonded to C(4′) of the two terpyridyl ligands is 6.9 Å.

transferred from the metal-centered orbital is localized on one of the terpyridyl ligands.[14,48]

At the outset, addition of DMSO molecules to $[Fe(terpy)_2]^{2+}$ has a small effect on E_{op}. The values of E_{op} for $n = 1-5$ are between 18616 and 18702 cm^{-1}. Examination of the space-filling model for $[Fe(terpy)_2]^{2+}$ (Figure 4) reveals gaps or pockets between the ligands and partial exposure of the Fe^{II} center to the solvent. Space-filling models for the complex and dimethyl sulfoxide generated with MacroModel[56] indicate that there is sufficient room for the first four DMSO molecules to sit deeply enough in the gaps to interact with the metal center as well as the ligand π-system. Molecular mechanics simulations using MacroModel's MM2* force field with Monte Carlo energy minimization for clusters with $n = 4$ and 8 place the first three or four DMSO molecules in the interligand pockets with their oxygen atoms oriented toward the Fe^{II} center. Precedent for small molecules occupying the pockets between the ligands in this complex is provided by the X-ray crystal structure for $[Fe(terpy)_2](ClO_4)_2 \cdot H_2O$, where the perchlorate anions and water occupy this space.[55] In development of an ellipsoidal cavity-dielectric continuum model to describe solvent reorganization accompanying MMCT, Brunschwig et al.[20] comment that the effective radius of the cavity is reduced in complexes containing the polypyridine ligand bipyridine because solvent can occupy the space between the ligands.

The DMSO molecules that occupy the interligand pockets reduce the energy of the ground state by interacting strongly with the charge residing on the metal ion and the portion delocalized onto the ligands. In the excited state, an electron is transferred to one of the ligand π^* molecular orbitals, leaving the metal formally in the +3 oxidation state and creating a net dipole moment. Stabilization of the excited-state charge distribution by DMSO molecules in direct contact with $[Fe(terpy)_2]^{2+}$ is comparable to stabilization of the ground state, resulting in little change in E_{op} for the first few DMSO molecules added. In fact, the initial increase in E_{op} with the addition of the second and third DMSO molecules either reflects a slightly stronger stabilization of the ground state with addition of these solvent molecules or differences in cluster temperatures, which are anticipated to decrease with increasing cluster size.[46] Metastable decay fractions[61] corresponding to loss of one DMSO from mass-selected $[Fe(terpy)_2 \cdot (DMSO)_n]^{2+}$ clusters are below 0.10 for $n = 1-3$ and between 0.10 and 0.15 for $n = 4-5$, which is consistent with a strong interaction between these first five DMSO molecules and $[Fe(terpy)_2]^{2+}$. For comparison, the metastable decay fractions for $n = 8-10$ jump to nearly 0.40. There is an apparent transition in metastable decay behavior around $n = 6$ or 7, where the respective metastable decay fractions are 0.24 and 0.11.

As the next several DMSO molecules, $n = 6-8$, are added, the anticipated red shift toward the bulk limit begins, with reorganization energies for individual solvent molecules ranging from -87 ± 31 cm^{-1} to -119 ± 30 cm^{-1}. For comparison, Blackbourn and Hupp[39] estimated a solvent reorganization energy of 125−150 cm^{-1} per first-shell DMSO molecule from a study of MMCT in mixed acetonitrile/DMSO solutions, where DMSO preferentially solvates the mixed-valence dimer. The positions in the interligand pockets in closest proximity to the metal ion are already occupied when the sixth through eighth DMSO molecules are added. As a consequence, these solvent molecules interact primarily with the terpyridyl ligands. The stabilizing effect of these solvent molecules on the ground-state charge distribution is diminished, while these solvent molecules continue to have a strong stabilizing effect on the charge transferred to the terpyridyl ligand in the photoinitiated ET process. Molecular modeling indicates that there is sufficient room for at least eight DMSO molecules to have close contact with the $[Fe(terpy)_2]^{2+}$ complex. Addition of the ninth DMSO molecule to the cluster shifts E_{op} to the blue rather than continuing the trend toward lower energy. One possible explanation is that accommodation of the ninth DMSO molecule in the first solvent shell crowds the solvent, pushing the DMSO molecule(s) closest to the Fe^{II} ion even closer to enhance stabilization of the ground state. As the 10th and 11th DMSO molecules are added, E_{op} begins once again to shift to lower energy. However, the shift between $n = 10$ and $n = 11$ is much smaller than the sequential shifts observed between $n = 5$ and $n = 8$, which is consistent with closing of the first solvent-shell.

Development of a Cluster-Size Equation for E_{op} and the Approach to Bulk Behavior. The approach of E_{op} to the bulk limit as well as deviations of E_{op} from the predictions of a dielectric continuum model, which are indicative of specific solvent interactions, will now be examined following the approach developed by Jortner and Rips[62,63] to model the cluster-size dependence of properties including vertical electron detachment energies,[64,65] ionization potentials, dispersive spectral shifts, and binding energies. Jortner has shown that the cluster-size dependence of these properties can be described by applying a correction, $C(n)$, to the bulk value $E(\infty)$ to account for the volume of the bulk absent in the cluster,

$$E(n) = E(\infty) - C(n) \qquad (4)$$

In the resulting cluster-size equation (CSE), the molecular-level interactions, which are difficult to handle computationally, are

included in the bulk value. The term correcting for the excluded volume contains the long-range interactions, which can be predicted using a dielectric continuum model.

Application of Jortner's approach to the cluster-size dependence of E_{op} for MLCT in $[Fe(terpy)_2]^{2+}$ requires determination of an appropriate correction term $C(n)$. The long-range interactions between ground state $[Fe^{II}(terpy)_2]^{2+}$, which has no net dipole moment, and DMSO are ion−dipole in nature. Excitation of the MLCT transition transfers an electron from the metal center to one of the ligands creating a polar excited state. When the complex is in its MLCT excited state, the long-range ion−dipole interactions between the complex and solvent remain essentially unchanged; however, new dipole−dipole interactions between the solvent and $[Fe^{III}(terpy^-)(terpy)]^{2+}$ stabilize the excited state relative to the ground state. Meyer and co-workers[14] used Kirkwood's equation[15] for the mutual electrostatic energy of an ion in a polar medium to derive the following expression for the solvent reorganization associated with MLCT in the related ions $[M^{II}(bpy)_3]^{2+}$ (M = Ru, Os):

$$E_{out} = \frac{\vec{\mu}_{es}^2}{b^3}\left[\frac{1 - D_{op}}{2\,D_{op} + 1}\right] \tag{5}$$

where $\vec{\mu}_{es}$ is the excited-state dipole moment, b is the effective radius of the ion, and D_{op} is the optical dielectric constant, which describes the response of the solvent medium to a high-frequency electric field.[66] In a dense isotropic medium, $(1 - D_{op})/(2\,D_{op} + 1)$ is directly proportional to the number density of polarizable electrons and the polarizability of these electrons.[67]

The same expression can be used to correct for the electrostatic energy of the ion that is absent when the region outside the cluster is excluded by replacing b with the cluster radius R_c

$$C(R_c) = \frac{\vec{\mu}_{es}^2}{R_c^3}\left[\frac{1 - D_{op}}{2\,D_{op} + 1}\right] \tag{6}$$

to yield. It is assumed in this approach that the dielectric constant within the cluster is unity. Using the expression for the cluster volume

$$V_c = ({}^4/_3)\pi R_c^3 = n({}^4/_3)\pi R_o^3 + ({}^4/_3)\pi b^3 \tag{7}$$

where R_o is the effective radius of a DMSO molecule and b is the effective radius of $[Fe(terpy)_2]^{2+}$, the correction term $C(R_c)$ can be expressed as a function of the cluster size n. The effective radius of DMSO determined from its density at 20 °C (1.1014 g cm^3)[68] is 3.041 Å. The space-filling model for $[Fe(terpy)_2]^{2+}$ generated with MacroModel yields a volume of 377 Å^3 and an effective radius of 4.48 Å. Since the space-filling model for DMSO generated by MacroModel yields a volume that is only 62% of that based on the density of DMSO, we scaled the volume for $[Fe(terpy)_2]^{2+}$ obtained from MacroModel by the same factor to get a molecular volume of 608 Å^3 and an effective radius b = 5.25 Å. This value is more consistent with the effective radius of 6.5 Å for $[Ru(bpy)_3]^{2+}$ and $[Os(bpy)_3]^{2+}$ used by Meyer and co-workers.[14] When the chromophore differs from the rest of the cluster constituents, the volume of the chromophore is typically ignored in developing CSE's.[62] However, it is unreasonable to neglect the volume occupied by the chromophore in this work because it is much larger than the solvent molecules and contributes appreciably to the cluster volume at small cluster sizes. Instead, the size of the complex is taken into account by introducing the factor b^3/R_o^3 when expressing the cluster radius R_c as a function of cluster size n

$$R_c^3 = nR_o^3 + b^3 = R_o^3\left(n + \frac{b^3}{R_o^3}\right) = R_o^3 n' \tag{8}$$

As a consequence,

$$C(n) = \frac{\vec{\mu}_{es}^2}{R_o^3 n'}\left(\frac{1 - D_{op}}{2D_{op} + 1}\right) \tag{9}$$

and

$$E_{op}(n) = E_{op}(\infty) - \frac{\vec{\mu}_{es}^2}{R_o^3 n'}\left[\frac{1 - D_{op}}{2D_{op} + 1}\right] \tag{10}$$

This cluster-size equation predicts that E_{op} is a function of $(n')^{-1}$, where $n' = n + b^3/R_o^3$.

Comparison of the predictions of the CSE with the values of E_{op} measured for MLCT in $[Fe(terpy)_2\cdot(DMSO)_n]^{2+}$, $n = 1-11$, requires knowledge of $E_{op}(\infty)$, D_{op}, and $\vec{\mu}_{es}$. In bulk solution, E_{op} is $(1.793 \pm 0.002) \times 10^4$ cm^{-1} and $D_{op} = 2.1815$ at 20 °C.[68] The excited-state dipole moment $\vec{\mu}_{es}$ can be determined from the solvent dependence of E_{op} in bulk solution (eq 5). A plot of E_{op} for $[Fe(terpy)_2]^{2+}$ in acetone, acetonitrile, dimethyl sulfoxide, dimethylformamide, methanol, and pyridazine solutions vs $(1 - D_{op})/(2\,D_{op} + 1)$ yields a slope of 3.687×10^3 cm^{-1} and an intercept of 1.876×10^4 cm^{-1}.[69] The slope corresponds to $\vec{\mu}_{es}^2/b^3$; the excited-state dipole moments determined for several values of b between 5.0 and 6.0 Å (Table 2) range from 9.57 to 12.6 D. Letting $b = 5.25$ Å yields $\vec{\mu}_{es} = 10.3$ D and $n' = n + 5.15$. In Figure 5a the experimentally determined values of E_{op} are plotted as a function of $(n + 5.15)^{-1}$ with the cluster-size dependence of E_{op} predicted by eq 10. At small cluster sizes there is significant deviation from the predictions of the CSE, as anticipated,[62] reflecting the specific solvent interactions with the $[Fe(terpy)_2]^{2+}$; however, there is essentially quantitative agreement for $n = 10, 11$.

The difference between the values of E_{op} measured for $[Fe(terpy)_2\cdot(DMSO)_n]^{2+}$ clusters and the predictions of the CSE summarized in Table 3 reflect the influence of molecular interactions in small clusters. Cluster-size equations provide a means for quantifying specific solvent interactions in excess of the electrostatic interactions between the dipole moment of the ET excited state and the polarizable electrons of the solvent. For clusters $n = 3-6$, the measured values of E_{op} exceed the CSE values by over 200 cm^{-1}. The experimental values for $n = 8, 10, 11$ begin to approach the CSE values, suggesting that a regime has been entered where specific solvent effects are no longer significant. Because of the uncertainty in determining an effective radius b for the $[Fe(terpy)_2]^{2+}$ complex, CSE's were determined for four values of b in the range 5.0−6.0 Å. The calculated excited-state dipole moments, values of n', and

TABLE 2: Cluster-Size Equation Parameters

b, Å	μ, D	n'	$\frac{-\vec{\mu}_{es}^2}{R_o^3}\left(\frac{1 - D_{op}}{2D_{op} + 1}\right)$, × 10^{-3} cm^{-1}
5.00	9.57	$n + 4.44$	3.61
5.25	10.3	$n + 5.15$	4.18
5.50	11.0	$n + 5.92$	4.81
6.00	12.6	$n + 7.68$	6.24

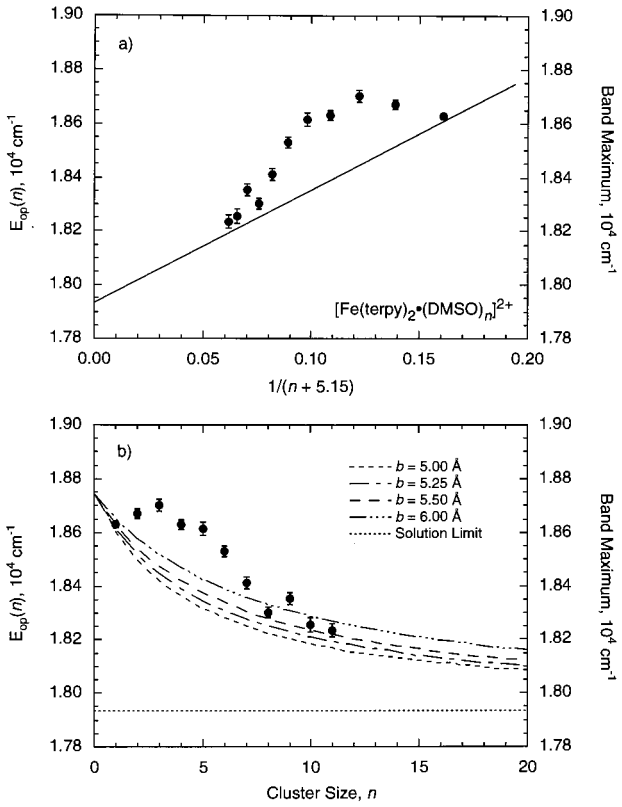

Figure 5. (a) MLCT absorption band maxima of $[Fe(terpy)_2 \cdot (DMSO)_n]^{2+}$ clusters monitored by photodepletion plotted as a function of $(n + 5.15)^{-1}$ for comparison with the predictions of the cluster-size equation (CSE) developed in the text (eq 10), assuming an effective chromophore radius of $b = 5.25$ Å for $[Fe(terpy)_2]^{2+}$; (b) $E_{op}(n)$ predicted by the CSE for several values of the effective chromophore radius b and the experimentally determined cluster band maxima shown as a function of cluster size, n.

corresponding values of $-(\vec{\mu}_{es}^2/R_o^3)[(1 - D_{op})/(2D_{op} + 1)]$ for eq 10 are summarized in Table 2. In Figure 5b, the CSE's for the four values of b are shown as a function of n with the measured values of E_{op}. Changing b has a small effect on the magnitude of the calculated E_{op}. The experimental data for $[Fe(terpy)_2 \cdot (DMSO)_n]^{2+}$ clusters begin to converge with the curve for $b = 5.50$ Å for clusters containing as few as 10 or 11 DMSO molecules. The slope of E_{op} plotted as a function of n (Figure 3) also shows a noticeable decrease, suggestive of a shell closing, in the same cluster-size range. The quantitative agreement between the predictions of a CSE for MLCT based on a dielectric continuum model and our experimental data for clusters as small as $n = 10$, 11 provides additional experimental justification for computational approaches which predict E_{op} in the condensed phase by first determining the electrostatic interactions between first-shell solvent and the CT chromophore in its ground and excited states with explicit consideration of molecular structure and then calculating the solvent shift associated with transfer of the CT chromophore surrounded by one solvent shell from the gas phase to a dielectric continuum.[34−36]

It is not possible to directly measure E_{op} of the unsolvated complex in the gas phase with laser photofragmentation ass spectrometry because the energy of the MLCT transition is insufficient to dissociate one of the tridentate terpyridyl ligands from the complex. However, E_{op} for the unsolvated complex can be estimated from our cluster data. The trend in the cluster-size dependence of E_{op} as $n \rightarrow 0$ (Figure 3) suggests that E_{op} for $[Fe(terpy)_2]^{2+}$ may be as low as 1.860×10^4 cm^{-1}. Another estimate of E_{op} for the unsolvated ion can be obtained from Figure 5b, where the curves converge at $n = 0$ to the value of 1.876×10^4 cm^{-1}, the intercept value from E_{op} vs $(1 - D_{op})/(2D_{op} + 1)$ in bulk solution for different solvents.[69] In a related study of MLCT in $[Fe(terpy)_2]^{2+}$ clustered with a variety of solvents,[69] the band maxima for the $n = 1$ clusters fell between these two estimates with the exception of $[Fe(terpy)_2 \cdot (CH_3CN)]^{2+}$, where $E_{op} = 18816 \pm 17$ cm^{-1}. If we assume that E_{op} for $[Fe(terpy)_2]^{2+}$ falls in the range $(1.860-1.876) \times 10^4$ cm^{-1}, the solvent reorganization energy in bulk solution is between -6.7×10^2 and -8.3×10^2 cm^{-1}. Consequently, addition of the first 11 DMSO molecules to $[Fe(terpy)_2]^{2+}$ recovers 54−63% of the bulk solvent reorganization energy. The CSE developed for this system predicts that the next eleven DMSO molecules added to the cluster will contribute only 13−17% of the bulk solvent reorganization energy.

With a reasonable estimate of the MLCT transition energy for the gas-phase complex, it is now possible to make comparisons with some of the theoretical and experimental work on similar systems. Zerner and co-workers found in calculations that association of 10 water molecules with $[Ru(NH_3)_5(pyr)]^{2+}$ produced 75% of the gas phase to solution shift in E_{op} for MLCT; association of 15 water molecules yielded 94% of the shift. The results of our study are perhaps not as dramatic as those observed for this system because there is no opportunity for hydrogen bonding in the $[Fe(terpy)_2 \cdot (DMSO)_n]^{2+}$ clusters. Using an approach which combined ab initio MCSCF and INDO methods to determine gas-phase electronic excitation energies with Monte Carlo simulations to predict ground-state solvent structures, Zeng, Hush, and Reimers[35] found that only solvent molecules within 5 Å of the center of the $[Ru(NH_3)_5(pyr)]^{2+}$ complex had a significant impact upon the energy of the MLCT transition, which is consistent with our observations. Finally, the experimental studies of MMCT and MLCT in DMSO/acetonitrile mixtures by the groups of Hupp[37,39,40] and Curtis[38] clearly point to the first solvent shell as the origin of most of the solvent reorganization energy and highlight the importance of molecular-level interactions between CT chromophores and solvent.

Conclusions

The contributions of individual molecules in the first solvent shell to the solvent reorganization associated with photoinitiated ET in a coordination complex have been quantified for the first time by using gas-phase clusters to control the local solvent environment and eliminate the influence of the bulk solvent. This study shows that over half of the solvent reorganization energy in this system arises from interactions between the $[Fe(terpy)_2]^{2+}$ complex and dimethyl sulfoxide molecules in the

TABLE 3: Deviation of Measured MLCT Band Maxima E_{op} for $[Fe(terpy)_2 \cdot (DMSO)_n]^{2+}$ Clusters from the Predictions of the Cluster-Size Equation, Assuming $b = 5.25$ Å

n	ΔE, $\times 10^{-2}$ cm^{-1}	n	ΔE, $10^{-2} \times$ cm^{-1}	n	ΔE, $\times 10^{-2}$ cm^{-1}	n	ΔE, $\times 10^{-2}$ cm^{-1}
1	0.2	4	2.4	7	1.3	10	0.5
2	1.5	5	2.7	8	0.5	11	0.4
3	2.6	6	2.2	9	1.2		

first solvent shell. Furthermore, comparison of the experimentally determined cluster-size dependence of E_{op} for MLCT with the predictions of a cluster size equation[62,63] developed for this system illustrates the effects of molecular-level solvent−solute interactions.

In more general terms, this work also clearly demonstrates the power of coupling electrospray ionization with laser photofragmentation mass spectrometry to probe the spectroscopy of species containing transition-metal ions in the chemically important +2 formal oxidation state, which have previously eluded spectroscopic study in the gas phase. Comparison of the electronic structure and reactivity of coordination complexes in the gas phase with their condensed-phase counterparts to make inferences regarding the role of solvent depends on the transition-metal ion having the same oxidation state in the gas and condensed phases. The presence of a strong absorption feature in the photodepletion action spectra of $[Fe(terpy)_2 \cdot (DMSO)_n]^{2+}$ clusters within 800 cm^{-1} of the band assigned to MLCT in solution confirms that this is the situation when this coordination complex is transferred to the gas phase by ESI.

Acknowledgment. Support for this work from NSF (Grant CHE-9616606) and Research Corporation (Cottrell Scholar Award) is gratefully acknowledged.

References and Notes

(1) Creutz, C. *Prog. Inorg. Chem.* **1983**, *30*, 1.
(2) Meyer, T. J. *Prog. Inorg. Chem.* **1983**, *30*, 389.
(3) Barbara, P. F.; Meyer, T. J.; Ratner, M. A. *J. Phys. Chem.* **1996**, *100*, 13148.
(4) Marcus, R. A. *Annu. Rev. Phys. Chem.* **1964**, *15*, 155.
(5) Marcus, R. A. *J. Chem. Phys.* **1956**, *24*, 966.
(6) Marcus, R. A. *J. Chem. Phys.* **1963**, *39*, 1734.
(7) Marcus, R. A. *J. Chem. Phys.* **1965**, *43*, 679.
(8) Hush, N. S. *Trans. Faraday Soc.* **1961**, *57*, 557.
(9) Levich, V. G.; Dogonadze, R. R. *Dokl. Akad. Nauk SSSR* **1959**, *124*, 123.
(10) Dogonadze, R. R. *Dokl. Akad. Nauk SSSR* **1960**, *133*, 1368.
(11) Dogonadze, R. R. *Dokl. Akad. Nauk SSSR* **1962**, *142*, 1108.
(12) Hush, N. S. *Prog. Inorg. Chem.* **1967**, *8*, 391.
(13) Hush, N. S. *Electrochim. Acta* **1968**, *13*, 1005.
(14) Kober, E. M.; Sullivan, B. P.; Meyer, T. J. *Inorg. Chem.* **1984**, *23*, 2098.
(15) Kirkwood, J. G. *J. Chem. Phys.* **1934**, *2*, 351.
(16) Hupp, J. T.; Meyer, T. J. *Inorg. Chem.* **1987**, *26*, 2332.
(17) Lewis, N. A.; Obeng, Y. S.; Purcell, W. L. *Inorg. Chem.* **1989**, *28*, 3796.
(18) McManis, G. E.; Gochev, A.; Nielson, R. M.; Weaver, M. J. *J. Phys. Chem.* **1989**, *93*, 7733.
(19) Hupp, J. T.; Dong, Y.; Blackbourn, R. L.; Lu, H. *J. Phys. Chem.* **1993**, *97*, 3278.
(20) Brunschwig, B. S.; Ehrenson, S.; Sutin, N. *J. Phys. Chem.* **1986**, *90*, 3657.
(21) Callahan, R. W.; Meyer, T. J. *Chem. Phys. Lett.* **1976**, *39*, 82.
(22) Callahan, R. W.; Keene, F. R.; Meyer, T. J.; Salmon, D. J. *J. Am. Chem. Soc.* **1977**, *99*, 1064.
(23) Curtis, J. C.; Sullivan, B. P.; Meyer, T. J. *Inorg. Chem.* **1983**, *22*, 224.
(24) Bignozzi, C. A.; Chiorboli, C.; Indelli, M. T.; Rampi Scandola, M. A.; Varani, G.; Scandola, F. *J. Am. Chem. Soc.* **1986**, *108*, 7872.
(25) Chang, J. P.; Fung, E. Y.; Curtis, J. C. *Inorg. Chem.* **1986**, *25*, 4233.
(26) Fung, E. Y.; Chua, A. C. M.; Curtis, J. C. *Inorg. Chem.* **1988**, *27*, 1294.
(27) Blackbourn, R. L.; Hupp, J. T. *J. Phys. Chem.* **1990**, *94*, 1788.
(28) Lowery, M. D.; Hammack, W. S.; Drickamer, H. G.; Hendrickson, D. N. *J. Am. Chem. Soc.* **1987**, *109*, 8019.
(29) Blackbourn, R. L.; Hupp, J. T. *Chem. Phys. Lett.* **1988**, *150*, 399.
(30) Stavrev, K. K.; Zerner, M. C.; Meyer, T. J. *J. Am. Chem. Soc.* **1995**, *117*, 8684.
(31) Zeng, J.; Craw, J. S.; Hush, N. S.; Reimers, J. R. *J. Chem. Phys.* **1993**, *99*, 1482.
(32) Zeng, J.; Hush, N. S.; Reimers, J. R. *J. Chem. Phys.* **1993**, *99*, 1496.
(33) Zeng, J.; Hush, N. S.; Reimers, J. R. *J. Chem. Phys.* **1993**, *99*, 1508.
(34) Zeng, J.; Hush, N. S.; Reimers, J. R. *J. Phys. Chem.* **1995**, *99*, 10459.
(35) Zeng, J.; Hush, N. S.; Reimers, J. R. *J. Am. Chem. Soc.* **1996**, *118*, 2059.
(36) Zeng, J.; Hush, N. S.; Reimers, J. R. *J. Phys. Chem.* **1996**, *100*, 19292.
(37) Hupp, J. T.; Weydert, J. *Inorg. Chem.* **1987**, *26*, 2657.
(38) Ennix, K. S.; McMahon, P. T.; de la Rosa, R.; Curtis, J. C. *Inorg. Chem.* **1987**, *26*, 2660.
(39) Blackbourn, R. L.; Hupp, J. T. *J. Phys. Chem.* **1988**, *92*, 2817.
(40) Roberts, J. A.; Hupp, J. T. *Inorg. Chem.* **1992**, *31*, 157.
(41) Blackbourn, R. L.; Hupp, J. T. *Inorg. Chem.* **1989**, *28*, 3786.
(42) Curtis, J. C.; Blackbourn, R. L.; Ennix, K. S.; Hu, S.; Roberts, J. A.; Hupp, J. T. *Inorg. Chem.* **1989**, *28*, 3791.
(43) Curtis, J. C.; Roberts, J. A.; Blackbourn, R. L.; Dong, Y.; Massum, M.; Johnson, C. S.; Hupp, J. T. *Inorg. Chem.* **1991**, *30*, 3856.
(44) Goodwin, H. A. *Coord. Chem. Rev.* **1976**, *18*, 293.
(45) Burns, T. D.; Spence, T. G.; Mooney, M. A.; Posey, L. A. *Chem. Phys. Lett.* **1996**, *258*, 669.
(46) Spence, T. G.; Burns, T. D.; Guckenberger, G. B., V.; Posey, L. A. *J. Phys. Chem. A* **1997**, *101*, 1081.
(47) Spence, T. G.; Burns, T. D.; Posey, L. A. *J. Phys. Chem. A* **1997**, *101*, 139.
(48) Braterman, P. S.; Song, J.-I.; Peacock, R. D. *Inorg. Chem.* **1992**, *31*, 555.
(49) Fink, D. W.; Ohnesorge, W. E. *J. Am. Chem. Soc.* **1969**, *91*, 4995.
(50) McCusker, J. K.; Walda, K. N.; Dunn, R. C.; Simon, J. D.; Magde, D.; Hendrickson, D. N. *J. Am. Chem. Soc.* **1993**, *115*, 298.
(51) Creutz, C.; Chou, M.; Netzel, T. L.; Okumura, M.; Sutin, N. *J. Am. Chem. Soc.* **1980**, *102*, 1309.
(52) Farley, J. W. *Rev. Sci. Instrum.* **1985**, *59*, 1834.
(53) Morgan, G.; Francis, H. B. *J. Chem. Soc.* **1937**, 1649.
(54) Siano, D. B.; Metzler, D. E. *J. Chem. Phys.* **1969**, *51*, 1856.
(55) Baker, A. T.; Goodwin, H. A. *Aust. J. Chem.* **1985**, *38*, 207.
(56) Mohamadi, F.; Richards, N. G. J.; Guida, W. C.; Liskamp, R.; Lipton, M.; Caufield, C.; Chang, G.; Hendrickson, T.; Still, W. C. *J. Comput. Chem.* **1990**, *11*, 440.
(57) Baggio-Saitovitch, E.; de Paoli, M. A. *Inorg. Chim. Acta* **1978**, *27*, 15.
(58) Krumholz, P. *Inorg. Chem.* **1965**, *4*, 612.
(59) Jensen, P. W.; Jørgensen, L. B. *J. Mol. Struct.* **1982**, *79*, 87.
(60) Tanabe, Y.; Sugano, S. *J. Phys. Soc. Jpn.* **1954**, *9*, 753.
(61) Spence, T. G. Ph.D. Thesis, Vanderbilt University, 1997.
(62) Jortner, J. *Z. Phys. D* **1992**, *24*, 247.
(63) Rips, I.; Jortner, J. *J. Chem. Phys.* **1992**, *97*, 536.
(64) Lee, G. H.; Arnold, S. T.; Eaton, J. G.; Sarkas, H. W.; Bowen, K. H.; Ludewigt, C.; Haberland, H. *Z. Phys. D.* **1991**, *20*, 9.
(65) Arnold, S. T.; Hendricks, J. H.; Bowen, K. H. *J. Chem. Phys.* **1995**, *102*, 39.
(66) Cox, P. A. *The Electronic Structure and Chemistry of Solids*; Oxford University Press: New York, 1987; pp 60−62.
(67) Davydov, A. S. *Quantum Mechanics*, 2nd ed.; Pergamon: New York, 1976; pp 424−425.
(68) Lide, D. R. *CRC Handbook of Chemistry and Physics*, 76th ed.; CRC Press: Boca Raton, FL, 1995.
(69) Spence, T. G.; Trotter, B. T.; Burns, T. D.; Posey, L. A. *J. Phys. Chem. A.* **1998**, *102*, 6101.